nature research

https://doi.org/10.1038/s41563-020-00821-3

Supplementary information

Dzyaloshinskii–Moriya-like interaction in ferroelectrics and antiferroelectrics

In the format provided by the authors and unedited

Supplementary Information for "Dzyaloshinskii-Moriya-like interaction in ferroelectrics and anti-ferroelectrics"

Hong Jian Zhao,[1] Peng Chen,[1] Sergey Prosandeev,[1] Sergey Artyukhin,[2] and Laurent Bellaiche[1]

[1] *Physics Department and Institute for Nanoscience and Engineering, University of Arkansas, Fayetteville, Arkansas 72701, USA*

[2] *Quantum Materials Theory, Istituto Italiano di Tecnologia, 16163 Genova, Italy.*

This Supplementary Information contains the following sections.

- Supplementary Discussion I – Definition of the **q** points and their modulations
- Supplementary Discussion II – Verifying the trilinear couplings
- Supplementary Discussion III – Non-collinear ferroelectricity in $Pmc2_1$ $BiFeO_3$ and $Pna2_1$ $BiInO_3$
- Supplementary Discussion IV – The nearest neighbor $\mathbf{D}'$ vectors
- Supplementary Discussion V – The one-to-one correspondence between magnetic and electric DMI
- Supplementary Discussion VI – Other possible mechanisms for DMI
- Supplementary Discussion VII – A comparison between spin cantings driven by magnetic DMI and inhomogenous dipole patterns driven by electric DMI

Supplementary Discussion I – Definition of the q points and their modulations

In 5-atom cubic perovskites with lattice vectors $\mathbf{a}$, $\mathbf{b}$ and $\mathbf{c}$ and reciprocal lattice vectors $\mathbf{a}^*$, $\mathbf{b}^*$ and $\mathbf{c}^*$, we define the $\mathbf{q}$ points and corresponding modulations in Supplementary Table I. By modulation associated with $\mathbf{q} = q_x\mathbf{a}^* + q_y\mathbf{b}^* + q_z\mathbf{c}^*$ (referred to as $\mathbf{q} = (q_x, q_y, q_z)$), we mean that for a given physical quantity (e.g., a vector $\mathbf{V}$), its component on the (l, m, n) site (defined by $\mathbf{R}_{lmn} = l\mathbf{a} + m\mathbf{b} + n\mathbf{c}$) is equal to $\mathbf{V}_{lmn} = \mathbf{V}e^{2\pi i(lq_x+mq_y+nq_z)}$. In Supplementary Fig. 1, we show the ABO_3 perovskites with the anti-phase and in-phase BO_6 tiltings about the z-axis (panels (b) and (c)). Practically, the anti-phase tiltings can be along the x, y or z direction, termed as ω_x^R, ω_y^R, and ω_z^R, respectively. Note that, the anti-phase tiltings have only one type of modulation, which is associated with the R point (note that the defining equality of this point is given in Supplementary Table I). In contrast, the in-phase tiltings can be modulated with respect to M_x, M_y, or M_z points (these points are also defined in Supplementary Table I); once the M_α point is chosen, the axis of the in-phase tilting has to be along α as well. In other words, the in-phase tiltings only includes three types, with the symbols $\omega_x^{M_x}$, $\omega_y^{M_y}$, and $\omega_z^{M_z}$, respectively. The ferroelectric and anti-ferroelectric symmetrized atomic motions are represented by the symbol d_α^K and given by $d_\alpha^K = \frac{1}{N}\sum_{lmn} e^{(i\mathbf{K}\cdot\mathbf{R}_{lmn})} r^d_{lmn,\alpha}$ with $r^d_{lmn,\alpha}$ being displacement of the ion initially located at $\mathbf{R}_{lmn} = l\mathbf{a}+m\mathbf{b}+n\mathbf{c}$, and N being the total number of 5-atom perovskite lattices. Here, $d = A$ or B indicates that the motion is within A or B sublattice; K or $\mathbf{K}$ denote the K point modulation (see, e.g., Γ, R, M_x, X_y points in Supplementary Table I); the α is the direction for such motions (i.e., x, y, or z orientations). Note that the M_β modulated anti-ferroelectric motions can be oriented along the α direction (i.e., α does not have to be equal to β, which is unlike the case for in-phase tilting). Such fact is also valid for the X_β modulation.

Supplementary Table I. The definition of $\mathbf{q}$ points and the corresponding modulations. The "+" and "-" signs on each site indicate that the physical quantities here are with "+" and "-" signs, respectively.

Γ	X_x	X_y	X_z
$\mathbf{q}$ = (0, 0, 0)	$\mathbf{q}$ = (1/2, 0, 0)	$\mathbf{q}$ = (0, 1/2, 0)	$\mathbf{q}$ = (0, 0, 1/2)
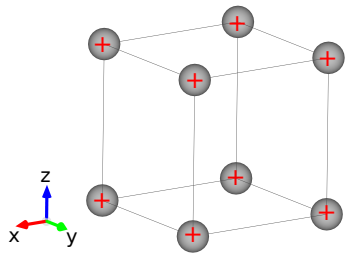	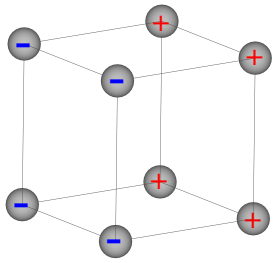	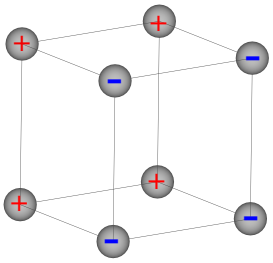	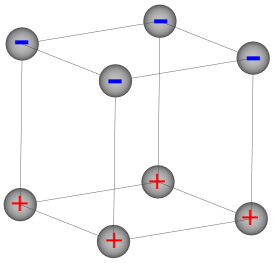
R	M_x	M_y	M_z
$\mathbf{q}$ = (1/2, 1/2, 1/2)	$\mathbf{q}$ = (0, 1/2, 1/2)	$\mathbf{q}$ = (1/2, 0, 1/2)	$\mathbf{q}$ = (1/2, 1/2, 0)
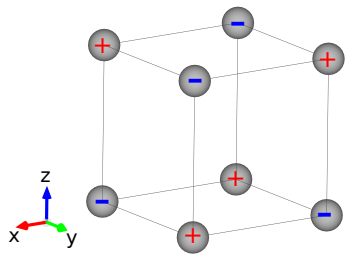	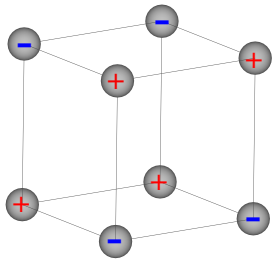	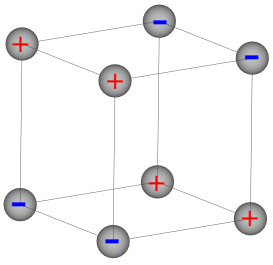	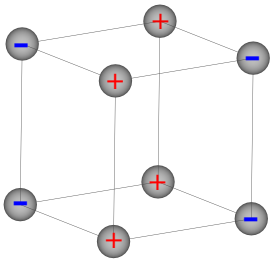

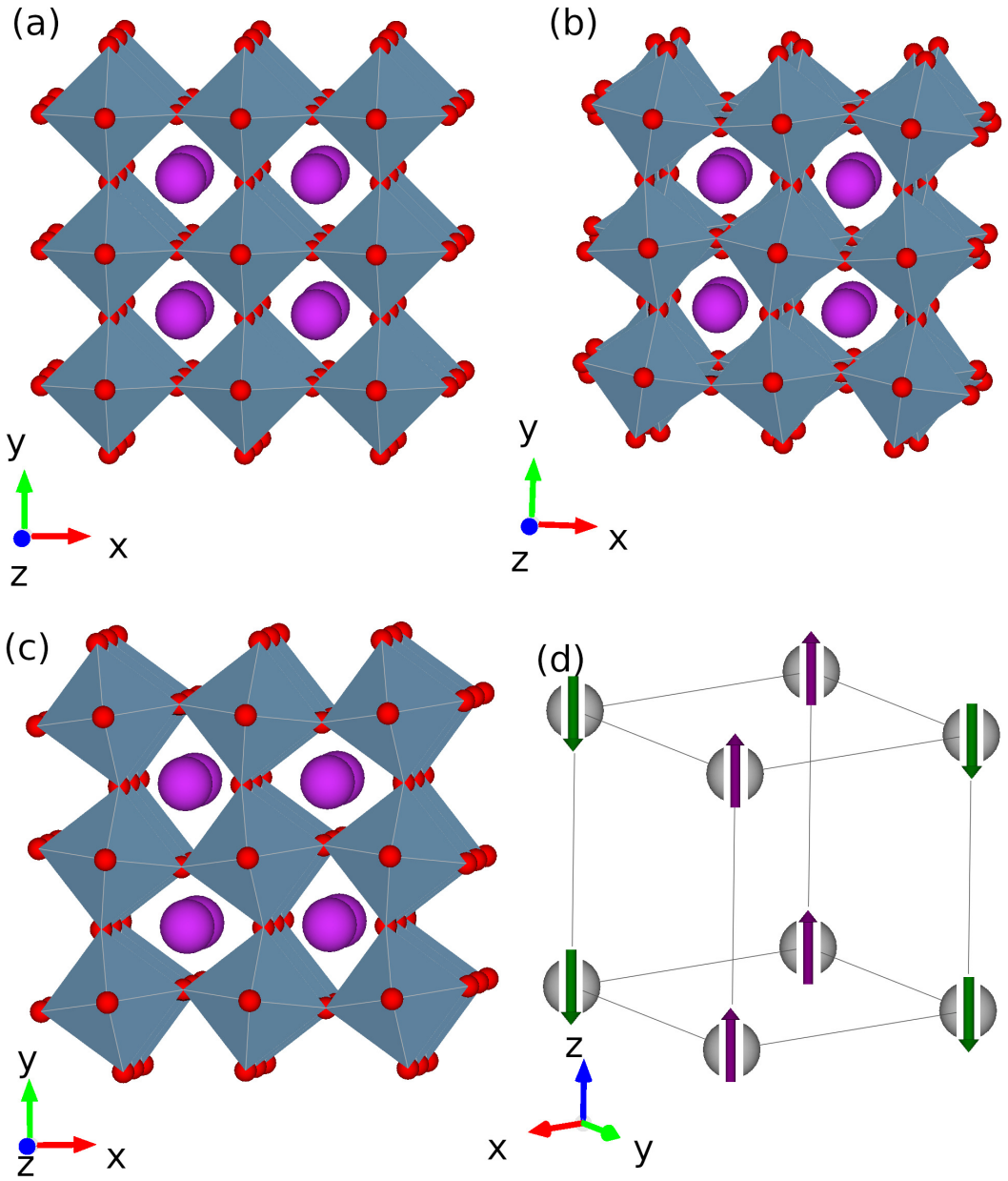

Supplementary Figure 1. The perovskites ABO_3 whose BO_6 octahedra is not tilted (panel (a)), tilted with anti-phase ω_z^R (panel (b)), and tilted with in-phase $\omega_z^{M_z}$ (panel (c)). In panel (d), we show a sketch for a physical quantity (e.g., vector **V** along the z direction) on A or B sublattices with M_z modulation. Note that the purple (along the $+z$ direction) and green (along $-z$ direction) arrows are centered on the sites with "+" and "-" signs sketched in Supplementary Table I for **q**=(1/2, 1/2, 0), respectively. If the arrows represent the tiltings on B sublattice, panel (d) will denote the in-phase tilting ($\omega_z^{M_z}$). Furthermore, the arrows can also represent the anti-ferroelectrics on A (respectively, B) sublattice, and panel (d) will then be linked with the symbols $A_z^{M_z}$ (respectively, $B_z^{M_z}$).

Supplementary Discussion II – Verifying the trilinear couplings

The additional data figure verifying the E_i ($i = 1 - 18$) in Table I of the main text and Supplementary Table II is shown as Supplementary Fig. 2.

Supplementary Table II. The six additional trilinear couplings (E_i with $i = 13 - 18$) not related to electric DMI. For our convention and definition of the symbols (e.g., $\epsilon_{\alpha\beta\gamma}$, $B_\beta^{X_\alpha}$), we refer to the caption of Table I of the main text. The purple and yellow balls denote the A and B ions, respectively. The corresponding motions are shown by red or cyan symbols in the summands and denoted by red or cyan arrows in the sketches. For clarity of the display, we adopt the cell centered on B ion.

$E_{13} \propto \epsilon_{\alpha\beta\gamma}\omega_\alpha^R B_\beta^{X_\alpha} A_\beta^{M_\alpha}$	$E_{14} \propto \epsilon_{\alpha\beta\gamma}\omega_\alpha^{M_\alpha} A_\beta^\Gamma A_\beta^{M_\alpha}$	$E_{15} \propto \epsilon_{\alpha\beta\gamma}\omega_\alpha^{M_\alpha} B_\beta^\Gamma A_\beta^{M_\alpha}$
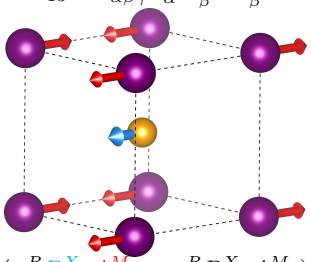	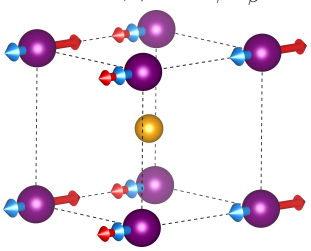	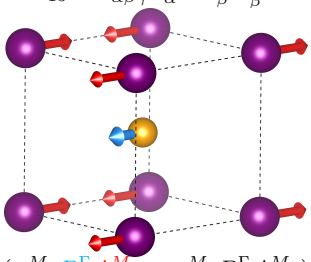
$(\omega_z^R B_x^{X_z} A_x^{M_z} - \omega_z^R B_y^{X_z} A_y^{M_z})$	$(\omega_z^{M_z} A_x^\Gamma A_x^{M_z} - \omega_z^{M_z} A_y^\Gamma A_y^{M_z})$	$(\omega_z^{M_z} B_x^\Gamma A_x^{M_z} - \omega_z^{M_z} B_y^\Gamma A_y^{M_z})$
Supplementary Fig. 2(k)	Supplementary Fig. 2(a)	Supplementary Fig. 2(b)
$E_{16} \propto \epsilon_{\alpha\beta\gamma}\omega_\alpha^{M_\alpha} A_\beta^R A_\beta^{X_\alpha}$	$E_{17} \propto \epsilon_{\alpha\beta\gamma}\omega_\alpha^{M_\alpha} A_\beta^{X_\beta} A_\beta^{X_\gamma}$	$E_{18} \propto \epsilon_{\alpha\beta\gamma}\omega_\alpha^{M_\alpha} A_\beta^{M_\beta} A_\beta^{M_\gamma}$
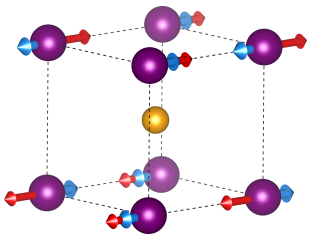	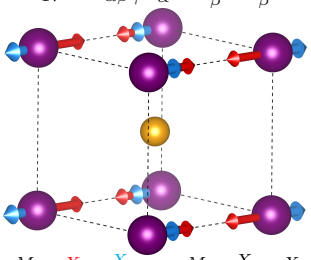	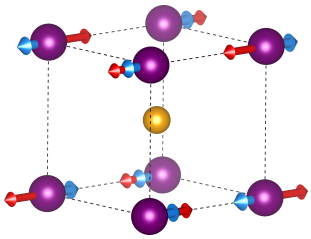
$(\omega_z^{M_z} A_x^R A_x^{X_z} - \omega_z^{M_z} A_y^R A_y^{X_z})$	$(\omega_z^{M_z} A_x^{X_x} A_x^{X_y} - \omega_z^{M_z} A_y^{X_y} A_y^{X_x})$	$(\omega_z^{M_z} A_x^{M_x} A_x^{M_y} - \omega_z^{M_z} A_y^{M_y} A_y^{M_x})$
Supplementary Fig. 2(e)	Supplementary Fig. 2(f)	Supplementary Fig. 2(c)

Supplementary Discussion III – Non-collinear ferroelectricity in $Pmc2_1$ $BiFeO_3$ and $Pna2_1$ $BiInO_3$

Let us first indicate that we also found six additional couplings in the form of $\sum_{\alpha\beta\gamma} \epsilon_{\alpha\beta\gamma}\omega_\alpha Q_{1,\beta} Q_{2,\beta}$ (with α being different from β, along with α and β being x, y or z), which are by-products when searching for the terms listed in Table I of the main text. These mechanisms (summarized in Supplementary Table II) result in *collinear* ferroelectricity or anti-ferroelectricity when considering a single of such terms (i.e., the motions Q_1 and Q_2 are both along the same single direction in Cartesian coordinate system). In contrast, when Q_1 and Q_2 are along multiple directions (e.g., $(Q_{1,x}, Q_{1,y})$ or $(Q_{2,x}, -Q_{2,y})$), non-collinear ferroelectricity or anti-ferroelectricity can be obtained when considering several of these terms. Let us take the E_{14} mechanism as an example, assuming that the in-phase tiltings are along the z direction ($\omega_z^{M_z}$), and the Γ-point ferroelectric motions are along $x + y$ direction (A_x^Γ and A_y^Γ). As a result, E_{14} automatically generates $A_x^{M_z}$ and $-A_y^{M_z}$. Consequently, the E_{14} mechanism can result in non-collinear motions (see Supplementary Fig. 3). The reason why we mention such fact here is that it plays an important role to interpret the non-collinear motions of A cations in the $Pmc2_1$ phase of e.g., $BiFeO_3$ [1].

The detailed structural analysis for strained $BiFeO_3$ within $Pmc2_1$ was done by Yang *et al.* [1]. We simply repeat the main results of Ref. [1] here: for both Bi and Fe ions, there are ferroelectric motions along the pseudo-cubic [110] direction (Supplementary Fig. 4(a)) and anti-ferroelectric motions along the pseudo-cubic [-110] direction associated with M_z point (z is along the pseudo-cubic [001] direction) (Supplementary Fig. 4(b)); the combination of ferroelectric and anti-ferroelectric motions renders non-collinear ferroelectric displacements for both Bi and Fe ions with "zigzag" pattern (Supplementary Fig. 4(c)) [1].

Regarding the $Pna2_1$ state $BiInO_3$ [2], a refined analysis clearly shows that In_1, In_2, In_3 and In_4 ions have the displacement vectors (i.e., $\mathbf{d}_{In}$ defined in Supplementary Fig. 4(e)) of (0.045, 0.006, 0), (0.045, -0.006, 0), (-0.045, 0.006, 0), and (-0.045, -0.006, 0) Å, respectively. Note that the (d_x, d_y, d_z) motions are expressed in the basis defined by the pseudo-cubic [110], [-110], and [001] directions, respectively. In other words, along the pseudo-cubic [-110] direction, there is a $R-$point modulated anti-ferroelectric motions (with a magnitude of 0.006 Å) for In ions; along the pseudo-cubic [110] direction, the anti-ferroelectric displacements (with the magnitude of 0.045 Å) of In is associated to the X_z point. Similarly, we can obtain the motions of Bi ions with respect to the "average" position of

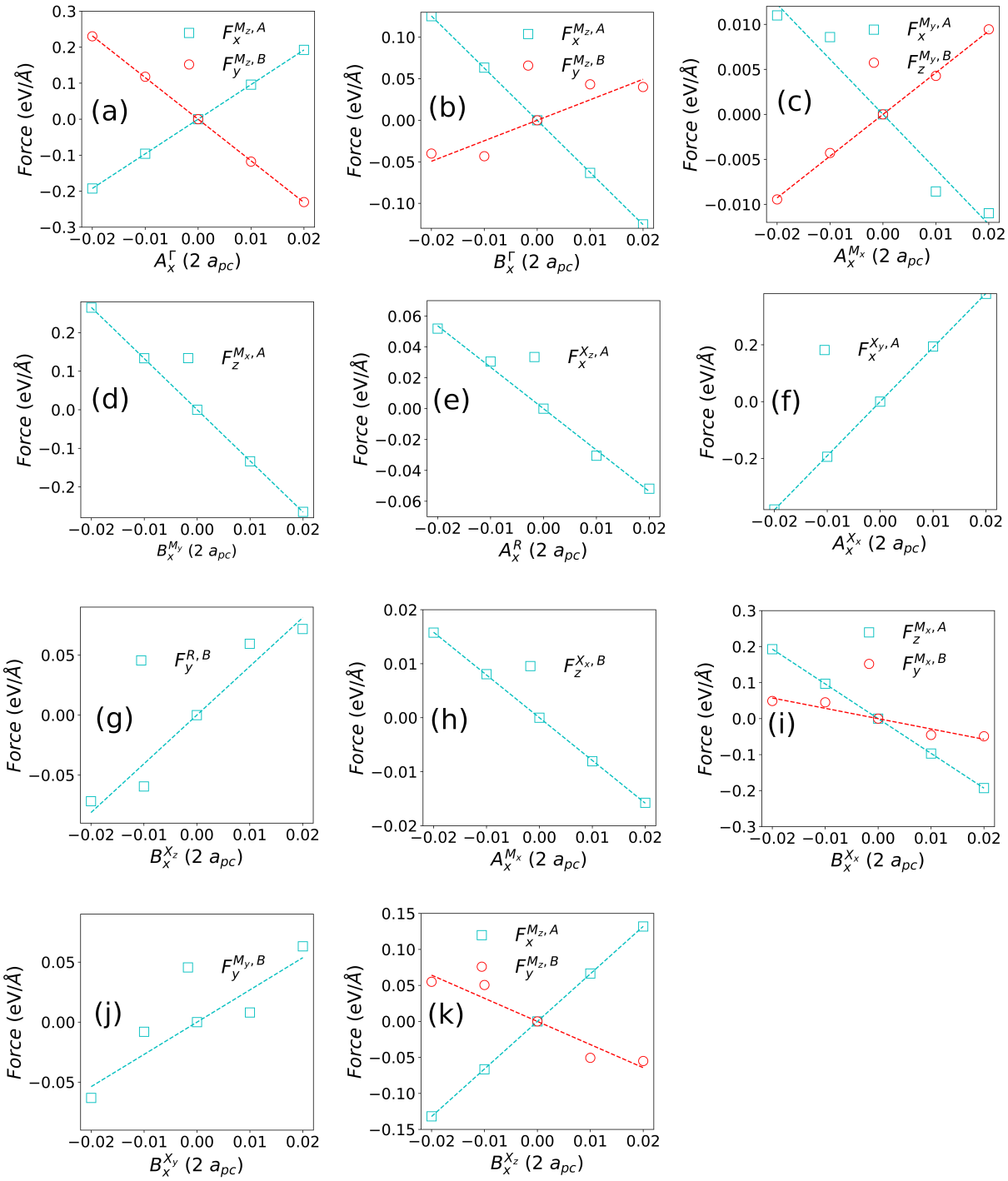

Supplementary Figure 2. The forces acting on Bi or Al ions when displacing Bi or Al ions associated with various modulations along the x direction. Here, the symbols "$F_\alpha^{K,d}$" in the legends denote the symmetrized forces (along the α direction) for Bi ($d = A$) or Al ($d = B$) ions associated with a K modulation, respectively. It is calculated by $F_\alpha^{K,d} = \frac{1}{N}\sum_{lmn} e^{(i\mathbf{K}\cdot\mathbf{R}_{lmn})} F_{lmn,\alpha}^{d}$ where $F_{lmn,\alpha}^{d}$ is the force acting on d ion for $(l,n,m)_{th}$ lattice ($\mathbf{R}_{lmn} = l\mathbf{a} + m\mathbf{b} + n\mathbf{c}$), and N is the total number of lattices. In panels (a) – (g) and (h) – (k), the in-phase $\omega_z^{M_z}$ and anti-phase ω_z^{R} tiltings are fixed as about 8^o, respectively.

O ions surrounding it. Interestingly, BiO_6 octahedral is formed in $BiInO_3$ as well but with much heavier distortion

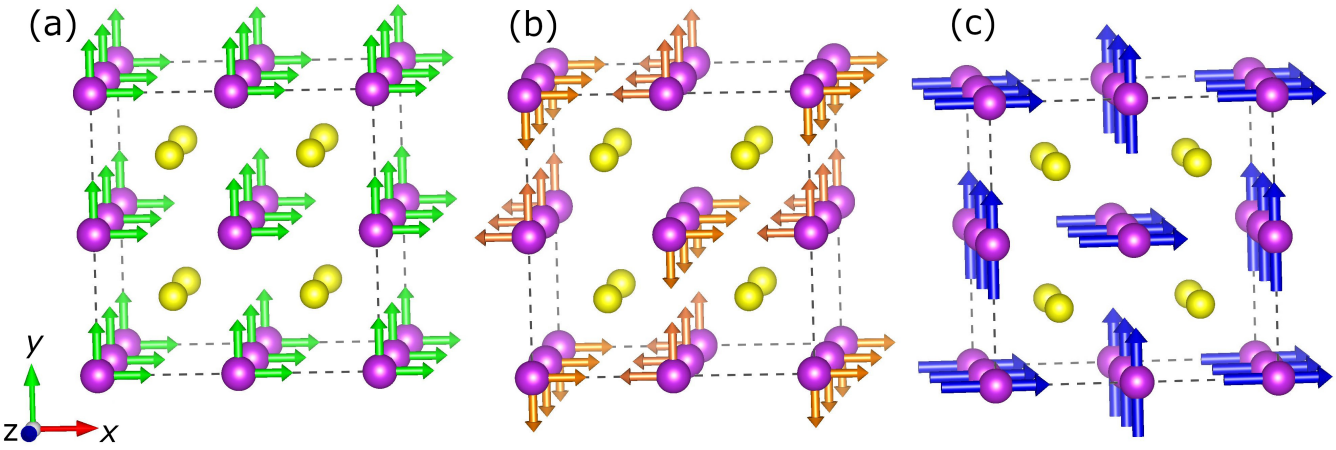

Supplementary Figure 3. Sketches for the ferroelectric and anti-ferroelectric motions for A ions in ABO_3 perovskites; the A and B ions are represented by purple and yellow balls. Panels (a) and (b) are ferroelectric motions (along $x+y$ direction) and anti-ferroelectric motions (along $x-y$ direction); panel (c) is the overall motions of A ions. We assume that the magnitudes of A^{Γ} and A^{M_z} are identical.

compared to InO_6 octahedral. We then identify three type of motions for Bi sublattice: ferroelectric motion of -0.45 Å along pseudo-cubic [001] direction (i.e., Bi_z^{Γ}), anti-ferroelectric motion of 0.19 Å along pseudo-cubic [110] direction (i.e. $\mathrm{Bi}_x^{X_z}$ and $\mathrm{Bi}_y^{X_z}$), and another anti-ferroelectric motion of 0.05 Å along pseudo-cubic [-110] direction (i.e., $-\mathrm{Bi}_x^{R}$ and Bi_y^{R}). The combination of $R-$point modulated anti-ferroelectric motions for In and $\Gamma-$point ferroelectric motions for Bi forms non-collinear ferroelectricity of $BiInO_3$, as interpreted by our E_7 term in Table I of the main text.

Finally, there are three types of motions in $BiInO_3$ that can not be explained by our terms in Table I. The first type is the X_z-point modulated motions for Bi ions (i.e. $\mathrm{Bi}_x^{X_z}$ and $\mathrm{Bi}_y^{X_z}$), which, in fact, originates from the trilinear coupling involving two tiltings rather than a single one ($\omega_{xy}^{R}\omega_{z}^{M_z}A_{xy}^{X_z}$, A =Bi) [3, 4] where ω_{xy}^{R}, $\omega_{z}^{M_z}$, and $A_{xy}^{X_z}$ are InO_6's anti-phase tilting along xy-direction (i.e., pseudo-cubic [110], see Supplementary Fig. 4(f)), InO_6's in-phase tilting along z-direction, and Bi's anti-ferroelectric motions (X_z point) along xy-direciton. The second type is the R-point modulated motions for Bi ions (i.e., $-\mathrm{Bi}_x^{R}$ and Bi_y^{R}) which is explained by ($\omega_{xy}^{R}\omega_{z}^{M_z}\omega_{z}^{M_z}A_{\bar{x}y}^{R}$, A =Bi) [3, 4]. Note that $\omega_{xy}^{R}\omega_{z}^{M_z}A_{xy}^{X_z}$ and $\omega_{xy}^{R}\omega_{z}^{M_z}\omega_{z}^{M_z}A_{\bar{x}y}^{R}$ are closely related to the BO_6 octahedral-induced hybrid improper ferroelectricity in $A'BO_3/A''BO_3$ superlattices [5–9]. The third type is the X_z-point modulated motions for In ions (i.e., 0.045 Å along pseudo-cubic [110]) which is interpreted by a *four-term* coupling $\omega_{xy}^{R}\omega_{z}^{M_z}B_{xy}^{X_z}A_{z}^{\Gamma}$ (B=In, A=Bi). All these anti-ferroelectric motions of the Bi ions, combined with their ferroelectric motions, result in non-collinear ferroelectricity as well – indicating other interesting non-collinear-ferroelectric mechanisms that go beyond the trilinear couplings revealed in the main text (such other mechanisms may be studied in other works).

Supplementary Table III. The DMI of nearest neighbor $B_{i_x,i_y,i_z}-B_{j_x,j_y,j_z}$ pair driven by in-phase or anti-phase tiltings of BO_6 octahedra. The $\mathbf{D}'(x)$, $\mathbf{D}'(y)$, and $\mathbf{D}'(z)$ vectors are for $B_{i_x,i_y,i_z}-B_{i_x+1,i_y,i_z}$, $B_{i_x,i_y,i_z}-B_{i_x,i_y+1,i_z}$, and $B_{i_x,i_y,i_z}-B_{i_x,i_y,i_z+1}$ pairs, respectively (see Text).

Mechanisms	$\mathbf{D}'(x)$	$\mathbf{D}'(y)$	$\mathbf{D}'(z)$	Proportionality
E_1	$(\omega_x^R,\omega_y^R,\omega_z^R)$	$(\omega_x^R,\omega_y^R,\omega_z^R)$	$(\omega_x^R,\omega_y^R,\omega_z^R)$	$\propto(-1)^{i_x+i_y+i_z}$
E_2	$(\omega_x^R,0,0)$	$(0,\omega_y^R,0)$	$(0,0,\omega_z^R)$	$\propto(-1)^{i_x+i_y+i_z}$
E_3	$(\omega_x^R,0,0)$	$(0,\omega_y^R,0)$	$(0,0,\omega_z^R)$	$\propto(-1)^{i_x+i_y+i_z}$
E_4	$(-\omega_x^R,\omega_y^R,\omega_z^R)$	$(\omega_x^R,-\omega_y^R,\omega_z^R)$	$(\omega_x^R,\omega_y^R,-\omega_z^R)$	$\propto(-1)^{i_x+i_y+i_z}$
E_5	$(0,(-1)^{i_y}\omega_y^{M_y},(-1)^{i_z}\omega_z^{M_z})$	$((-1)^{i_x}\omega_x^{M_x},0,(-1)^{i_z}\omega_z^{M_z})$	$((-1)^{i_x}\omega_x^{M_x},(-1)^{i_y}\omega_y^{M_y},0)$	$\propto(-1)^{i_x+i_y+i_z}$
E_6	$(0,(-1)^{i_y}\omega_y^{M_y},(-1)^{i_z}\omega_z^{M_z})$	$((-1)^{i_x}\omega_x^{M_x},0,(-1)^{i_z}\omega_z^{M_z})$	$((-1)^{i_x}\omega_x^{M_x},(-1)^{i_y}\omega_y^{M_y},0)$	$\propto(-1)^{i_x+i_y+i_z+1}$

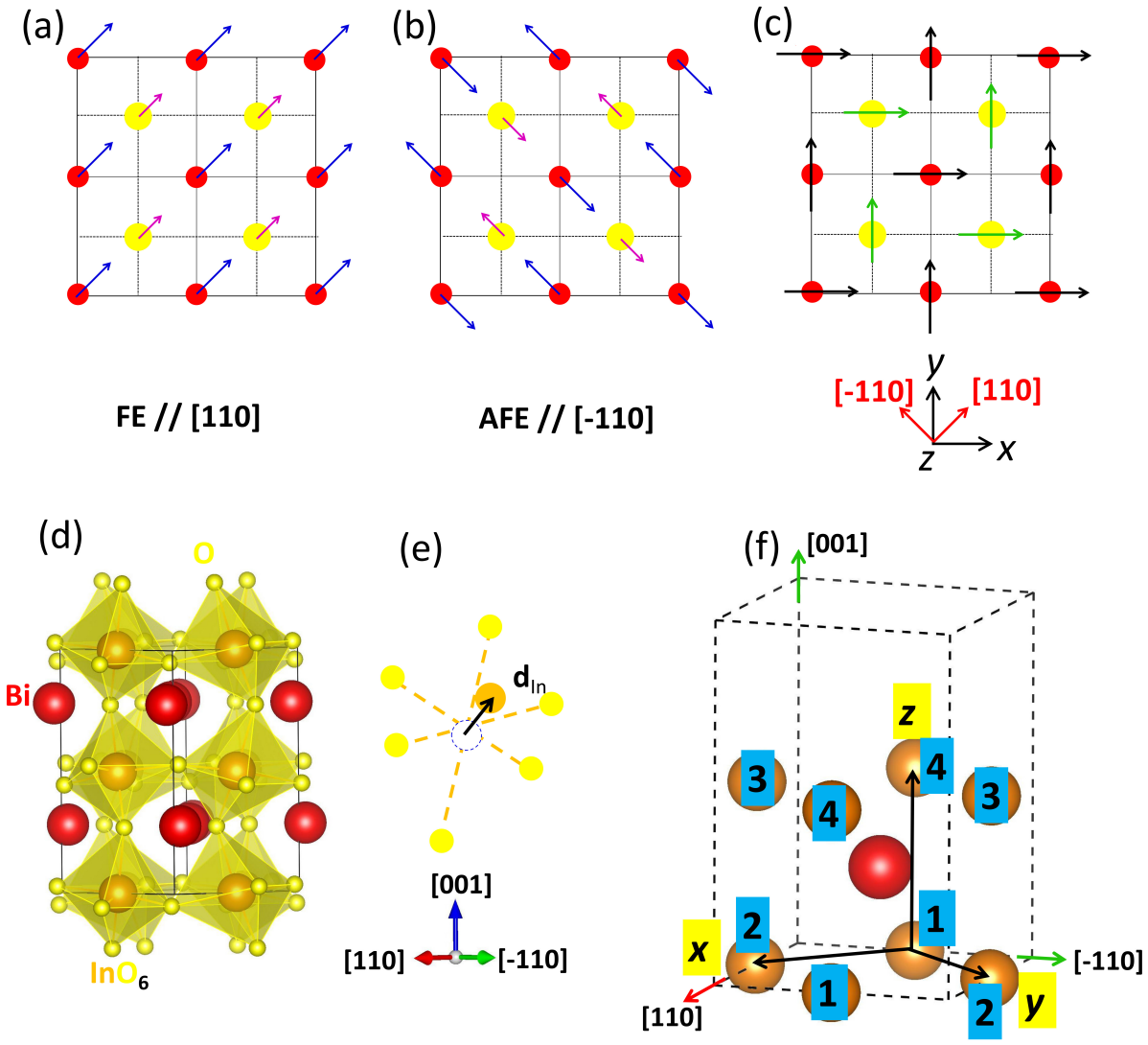

Supplementary Figure 4. The ferroelectric (FE) and anti-ferroelectric (AFE) motions for A and/or B ions in ABO_3 perovskites. Panels (a), (b), and (c) are sketches for the ferroelectric, anti-ferroelectric, and overall motions (denoted by arrows) of Bi (red circles) and Fe (yellow circles) ions in $BiFeO_3$. Note that Panels (a), (b), and (c) are reproduced by taking Ref. [1] as a reference (see its Fig. 3(b)). Panel (d) is the crystal structure of $Pna2_1$ $BiInO_3$. Panel (e) is the sketch of InO_6 octahedra where yellow circles denote O ion and orange circle denotes In ion; the dashed vacant circle denotes the "average" position of the six O ions forming the InO_6 octahedra; the arrow indicates the displacement vectors of In ion with respect to the "average" O potision. Panel (f) shows the positions of In and Bi ions in $Pna2_1$ crystallographic coordinate system (e.g., the [110], [-110], and [001] directions) and in pseudo-cubic coordinate system (e.g., the $xyz-$ Cartesian coordinate system.) The "1", "2", "3" and "4" in panel (c) label the In ions.

Supplementary Discussion IV – The nearest neighbor D′ vectors

We now aim at extracting the underlying electric Dzyaloshinskii-Moriya interaction (DMI) vector based on the twelve mechanisms summarized in Table I of the main text. In the present work, we highlight the nearest neighbor DMI for $B-B$, $A-A$, and $A-B$ pairs (sketched in Supplementary Fig. 5), involving in-phase or anti-phase tilting. For that, let us start from, e.g.,

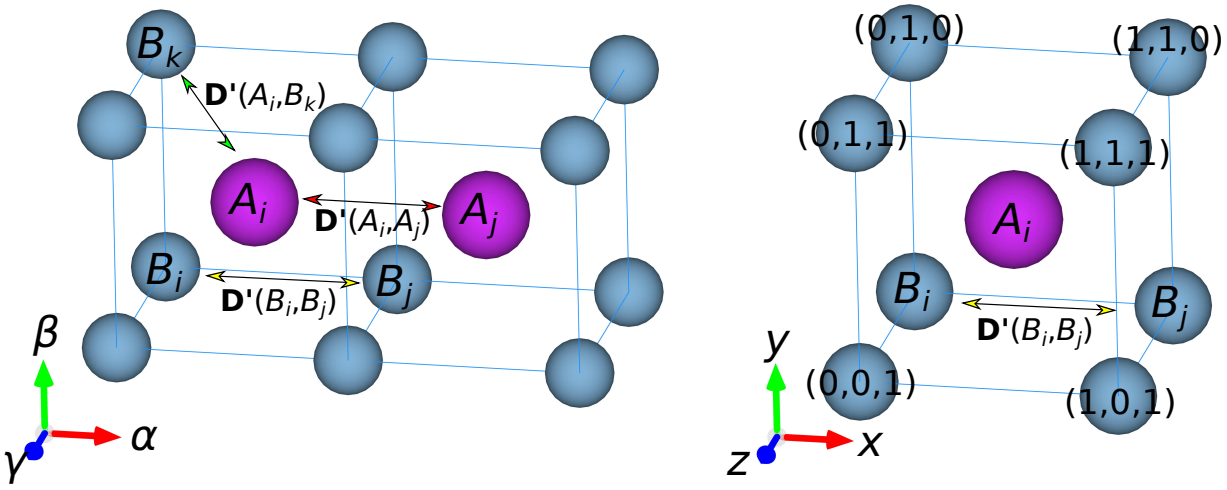

Supplementary Figure 5. Left panel: The DMI for the nearest neighbor $A-A$, $B-B$ and $A-B$ pairs in perovskite ABO_3, marked by $\mathbf{D}'(B_i,B_j)$, $\mathbf{D}'(A_i,A_j)$, and $\mathbf{D}'(A_i,B_k)$, respectively. When saying $\mathbf{D}'(B_i,B_j)$, $\mathbf{D}'(A_i,A_j)$, and $\mathbf{D}'(A_i,B_k)$, we are really meaning that the corresponding $\mathbf{D}'$ vectors are functions of $\mathbf{r}_{B_i}-\mathbf{r}_{B_j}$, $\mathbf{r}_{A_i}-\mathbf{r}_{A_j}$, and $\mathbf{r}_{A_i}-\mathbf{r}_{B_k}$, respectively. Here vector $\mathbf{r}$ denote the position vectors for A or B ions. For the DMI for nearest neighbor $A-A$ or $B-B$ pairs, the direction of $\mathbf{r}_{B_i}-\mathbf{r}_{B_j}$ or $\mathbf{r}_{A_i}-\mathbf{r}_{A_j}$ vectors, which is α in the left panel, can only be one of x, y, or z. Right panel: an explicit example showing the DMI for the nearest neighbor B_i-B_j pairs with $\mathbf{r}_{B_i}-\mathbf{r}_{B_j}$ along x direction. Note that, the i index is short for (i_x,i_y,i_z) with e.g., i_y denotes the index for i site along y direction. Following such convention, there are eight nearest neighbor A_i-B_k DMI, with k being $i+(0,0,0)$, $i+(1,0,0)$, $i+(0,1,0)$, $i+(0,0,1)$, $i+(1,1,0)$, $i+(1,0,1)$, $i+(0,1,1)$, and $i+(1,1,1)$, marked in the right panel. The unmarked B_i and B_j are recognized as $i+(0,0,0)$, and $i+(1,0,0)$, respectively.

$$E_1 \propto \sum_{\alpha\beta\gamma} \epsilon_{\alpha\beta\gamma}\omega^R_\alpha B^R_\beta B^\Gamma_\gamma \tag{S1}$$

Now the calculation process is done within a big supercell containing N 5-atom cells. We focus on the nearest neighbor DMI for $B-B$ pair with one B ion located at $i\equiv(i_x,i_y,i_z)$ site. Therefore the B^R_β, and B^Γ_γ can be written in the following way:

$$B^R_\beta = \sum_{j_x}\sum_{j_y}\sum_{j_z}(-1)^{j_x+j_y+j_z} r^B_{j_x,j_y,j_z,\beta}/N \tag{S2}$$

$$B^\Gamma_\gamma = \sum_{k_x}\sum_{k_y}\sum_{k_z} r^B_{k_x,k_y,k_z,\gamma}/N \tag{S3}$$

Inserting Eqs. S2 and S3 into Eq. S1, we then obtain $E_1 \propto \sum_{j,k}\sum_{\alpha\beta\gamma}\epsilon_{\alpha\beta\gamma}(-1)^{j_x+j_y+j_z}\omega^R_\alpha r^B_{j_x,j_y,j_z,\beta} r^B_{k_x,k_y,k_z,\gamma}/N^2$, where $j\equiv(j_x,j_y,j_z)$, and $k\equiv(k_x,k_y,k_z)$. In such supercell, one can define three nearest neighbor DMI vectors, i.e., $\mathbf{D}'(x)\equiv\mathbf{D}'_{i,i+(1,0,0)}$, $\mathbf{D}'(y)\equiv\mathbf{D}'_{i,i+(0,1,0)}$, and $\mathbf{D}'(z)\equiv\mathbf{D}'_{i,i+(0,0,1)}$, denoting the DMI for $B-B$ pairs along the x, y, and z directions, respectively. The z component of the $\mathbf{D}'(x)$ vector is given by Eq. S4 where $\delta_{(j_x,j_y,j_z),(i_x,i_y,i_z)} = \delta_{j_x,i_x}\delta_{j_y,i_y}\delta_{j_z,i_z}$.

$$\begin{aligned} D'(x)_z =& \frac{1}{2}\left(\frac{\partial^2 E_1}{\partial r^B_{i,x}\partial r^B_{i+(1,0,0),y}} - \frac{\partial^2 E_1}{\partial r^B_{i,y}\partial r^B_{i+(1,0,0),x}}\right) \propto \frac{1}{2}\sum_{j,k}\sum_{\alpha\beta\gamma}\epsilon_{\alpha\beta\gamma}(-1)^{j_x+j_y+j_z}\omega^R_\alpha \\ & [\delta_{\beta,x}\delta_{\gamma,y}\delta_{(j_x,j_y,j_z),(i_x,i_y,i_z)}\delta_{(k_x,k_y,k_z),(i_x+1,i_y,i_z)} + \delta_{\beta,y}\delta_{\gamma,x}\delta_{(j_x,j_y,j_z),(i_x+1,i_y,i_z)}\delta_{(k_x,k_y,k_z),(i_x,i_y,i_z)} \\ & -\delta_{\beta,y}\delta_{\gamma,x}\delta_{(j_x,j_y,j_z),(i_x,i_y,i_z)}\delta_{(k_x,k_y,k_z),(i_x+1,i_y,i_z)} - \delta_{\beta,x}\delta_{\gamma,y}\delta_{(j_x,j_y,j_z),(i_x+1,i_y,i_z)}\delta_{(k_x,k_y,k_z),(i_x,i_y,i_z)}] \\ =& 2(-1)^{i_x+i_y+i_z}\omega^R_z \end{aligned} \tag{S4}$$

We also have $D'(\chi)_\alpha \propto 2(-1)^{i_x+i_y+i_z}\omega_\alpha^R$ with χ and α being x, y or z. Using a similar strategy, we have obtained the DMI for the nearest neighbor $B-B$ (extracted from E_1 to E_6 mechanisms) and $B-A$ (extracted from E_7 to E_{12} mechanisms) pairs, summarized in Supplementary Tables III, IV, V, and VI respectively. The DMIs for $B-B$ and $A-B$ pairs are all driven by the anti-phase or in-phase tiltings of BO_6 octahedra. Given anti-phase tiltings along the χ direction (e.g., ω_χ^R, $\chi = x, y, z$), the DMI can be classified into longitudinal (e.g., $\mathbf{D}'(\chi)$) and transverse (e.g., $\mathbf{D}'(\chi')$, $\chi' = x, y, z$ but not equal to χ) cases. Obviously, from Supplementary Table III, the E_2 to E_4 mechanisms suggest the difference between $\mathbf{D}'(\chi)$ and $\mathbf{D}'(\chi')$. With in-phase tilting ω_χ^M, there are no longitudinal $\mathbf{D}'$; in other words, $\mathbf{D}'(\chi)_\chi$ is zero. Using ω^R and ω^M, the nearest neighbor $B_{i_x,i_y,i_z} - B_{j_x,j_y,j_z}$ pair's DMI can be written in a general form:

$$D'(\chi)_\eta \propto (-1)^{(i_x+i_y+i_z)}[K\omega_\eta^R\delta_{\chi,\eta} + K'\omega_\eta^R(1-\delta_{\chi,\eta}) + \kappa(1-\delta_{\chi,\eta})(-1)^{i_\eta}\omega_\eta^{M_\eta}] \tag{S5}$$

Similar to Eq. S2, the anti-phase and in-phase tiltings in supercell containing N 5-atom cells are defined by $\boldsymbol{\omega}^R = \sum_{lmn}(-1)^{(l+m+n)}\boldsymbol{\omega}_{lmn}/N$, $\omega_x^{M_x} = \sum_{lmn}(-1)^{(m+n)}\omega_{lmn,x}/N$, $\omega_y^{M_y} = \sum_{lmn}(-1)^{(l+n)}\omega_{lmn,y}/N$, and $\omega_z^{M_z} = \sum_{lmn}(-1)^{(l+m)}\omega_{lmn,z}/N$, respectively.

Interestingly, the DMI involving i and j sites is determined by $\boldsymbol{\omega}^R$ or $\boldsymbol{\omega}^M$ defined in the whole space (e.g., $\boldsymbol{\omega}^R = \frac{1}{N}\sum_{lmn}(-1)^{(l+m+n)}\boldsymbol{\omega}_{lmn}$) rather than those defined in a region localized around i and j sites. In other words, it seems that the DMI discussed here is driven by in-phase or anti-phase tilting in a non-localized way. Indeed, only the "simple" in-phase or anti-phase tiltings are considered to formulate the DMI in the present work. In fact, the tilting pattern of BO_6 can be more complicated than ω^R and ω^M. For example, in $NaNbO_3$, complex tilting pattern associated with $(1/2, 1/2, 1/4)$ has also been detected [10]. If we include the various non-Brillouin-zone-boundary related tilting modes (e.g., modes beyond R, M_x, M_y, and M_z), we may reach the DMI contributed by both localized and non-localized tiltings. On the other hand, if we interpret $\boldsymbol{\omega}^R$ or $\boldsymbol{\omega}^M$ in the basis localized around i and j sites, we will arrive at a localized contribution to $i-j$ pair's DMI.

Now let us compare our results with the $\mathbf{D}_{i,j} \propto K_{ij}(\boldsymbol{\omega}_i - \boldsymbol{\omega}_j)$ proposed in Refs. [11, 12] for magnetic DMI. We play with a $2\times2\times2$ supercell ($N = 8$) at (i_x, i_y, i_z) site and expand $\boldsymbol{\omega}^R$ by $\boldsymbol{\omega}^R = (-1)^{i_x+i_y+i_z}(\boldsymbol{\omega}^{i_x,i_y,i_z} - \boldsymbol{\omega}^{i_x+1,i_y,i_z} - \boldsymbol{\omega}^{i_x,i_y+1,i_z} - \boldsymbol{\omega}^{i_x,i_y,i_z+1} + \boldsymbol{\omega}^{i_x+1,i_y+1,i_z} + \boldsymbol{\omega}^{i_x+1,i_y,i_z+1} + \boldsymbol{\omega}^{i_x,i_y+1,i_z+1} - \boldsymbol{\omega}^{i_x+1,i_y+1,i_z+1})/8$. In first approximation (e.g., considering the nearest neighbors for $i \equiv (i_x, i_y, i_z)$ site only), the $\boldsymbol{\omega}^R$ can be written as $(-1)^{i_x+i_y+i_z}(\boldsymbol{\omega}^{i_x,i_y,i_z} - \boldsymbol{\omega}^{i_x+1,i_y,i_z})/2$, $(-1)^{i_x+i_y+i_z}(\boldsymbol{\omega}^{i_x,i_y,i_z} - \boldsymbol{\omega}^{i_x,i_y+1,i_z})/2$, and $(-1)^{i_x+i_y+i_z}(\boldsymbol{\omega}^{i_x,i_y,i_z} - \boldsymbol{\omega}^{i_x,i_y,i_z+1})/2$ when computing $\mathbf{D}'(x)$, $\mathbf{D}'(y)$, and $\mathbf{D}'(z)$, respectively. We further assume that in Eq. (S5), $K = K'$, $\kappa = 0$, and we have $\mathbf{D}'(x) \propto K(\boldsymbol{\omega}^{i_x,i_y,i_z} - \boldsymbol{\omega}^{i_x+1,i_y,i_z})/2$, $\mathbf{D}'(y) \propto K(\boldsymbol{\omega}^{i_x,i_y,i_z} - \boldsymbol{\omega}^{i_x,i_y+1,i_z})/2$, and $\mathbf{D}'(z) \propto K(\boldsymbol{\omega}^{i_x,i_y,i_z} - \boldsymbol{\omega}^{i_x,i_y,i_z+1})/2$; for the nearest neighbor $B_i - B_j$ pair's DMI, via some special assumptions, we thus have arrived at $\mathbf{D}'_{i,j} \propto K(\boldsymbol{\omega}_i - \boldsymbol{\omega}_j)$, which coincides with $\mathbf{D}_{i,j} \propto K_{ij}(\boldsymbol{\omega}_i - \boldsymbol{\omega}_j)$.

As for the nearest neighbor $A_{i_x,i_y,i_z} - B_{j_x,j_y,j_z}$ pair, the situation is more complicated compared to that of $B-B$ pair. This is quite easy to understand when realizing that the coordination number (CN) for $B-B$ and $A-B$ pairs are different (i.e., CN = 6 and CN = 8 for $B-B$ and $A-B$ pairs, respectively). In particular, the nearest neighbor $A-B$ pair is not along the x, y, or z directions, but along eight different $[l_x l_y l_z]$ orientations ($l_x, l_y, l_z = 0, 1$) with respect to cubic cell (see the caption of Supplementary Table IV for definition). From Supplementary Tables IV, V and VI, the DMI of $A_{i_x,i_y,i_z} - B_{j_x,j_y,j_z}$ pair, denoted by $D'(l_x, l_y, l_z)_\eta$, is summarized by the following equation:

$$\begin{aligned} D'(l_x, l_y, l_z)_\eta \propto (-1)^{(i_x+i_y+i_z)}[&(-1)^{l_x+l_y+l_z} I\omega_\eta^R + (-1)^{i_\eta}(-1)^{l_x+l_y+l_z+l_\eta} I'\omega_\eta^{M_\eta} + \\ &\iota\sum_{\beta\gamma} \mid \epsilon_{\eta\beta\gamma} \mid \omega_\beta^R(-1)^{l_\gamma} + \Lambda\sum_{\beta\gamma} \mid \epsilon_{\eta\beta\gamma} \mid \omega_\beta^{M_\beta}(-1)^{i_\beta+l_\beta+l_\gamma}] \end{aligned} \tag{S6}$$

Finally, none of our mechanisms (Table I in the main text and Supplementary Table II) hint towards the existence of a DMI for $A-A$ pairs. On the other hand, it is interesting that non-collinear ferroelectricity can also be achieved in a way going beyond DMI, that is not involving a cross-product between local displacements. For instance, in Supplementary Discussion III, we have shown that the E_{14} mechanism can result in non-collinear ferroelectricity. There are six such kinds of mechanisms (summarized in Supplementary Table II) having the form of $\sum_{\alpha\beta\gamma}\epsilon_{\alpha\beta\gamma}\omega_\alpha Q_{1,\beta}Q_{2,\beta}$, with α different from β; none of them is related to a cross product and thus none of them can be thought as being a DMI interaction.

Supplementary Table IV. The DMI of nearest neighbor $A_{i_x,i_y,i_z} - B_{j_x,j_y,j_z}$ pair driven by in-phase or anti-phase tiltings of BO_6 octahedra. There are eight B_{j_x,j_y,j_z} ions surrounding the A_{i_x,i_y,i_z} site; the sites for B ions are indexed by (l,m,n) where l, m and n are 0 or 1; the (l_x,l_y,l_z) for B_{j_x,j_y,j_z} sites denote that $j_x - i_x = l_x$, $j_y - i_y = l_y$, $j_z - i_z = l_z$ (see the right panel of Supplementary Fig. 5).

(l_x,l_y,l_z)	E_7 $\propto (-1)^{i_x+i_y+i_z}$	E_8 $\propto (-1)^{i_x+i_y+i_z}$	E_9 $\propto (-1)^{i_x+i_y+i_z}$
(0,0,0)	$(\omega_x^R, \omega_y^R, \omega_z^R)$	$((-1)^{i_x}\omega_x^{M_x}, (-1)^{i_y}\omega_y^{M_y}, (-1)^{i_z}\omega_z^{M_z})$	$(-\omega_y^R - \omega_z^R, -\omega_z^R - \omega_x^R, -\omega_x^R - \omega_y^R)$
(1,0,0)	$(-\omega_x^R, -\omega_y^R, -\omega_z^R)$	$((-1)^{i_x}\omega_x^{M_x}, -(-1)^{i_y}\omega_y^{M_y}, -(-1)^{i_z}\omega_z^{M_z})$	$(-\omega_y^R - \omega_z^R, \omega_z^R - \omega_x^R, -\omega_x^R + \omega_y^R)$
(0,1,0)	$(-\omega_x^R, -\omega_y^R, -\omega_z^R)$	$(-(-1)^{i_x}\omega_x^{M_x}, (-1)^{i_y}\omega_y^{M_y}, -(-1)^{i_z}\omega_z^{M_z})$	$(-\omega_y^R + \omega_z^R, -\omega_z^R - \omega_x^R, \omega_x^R - \omega_y^R)$
(0,0,1)	$(-\omega_x^R, -\omega_y^R, -\omega_z^R)$	$(-(-1)^{i_x}\omega_x^{M}, -(-1)^{i_y}\omega_y^{M}, (-1)^{i_z}\omega_z^{M})$	$(\omega_y^R - \omega_z^R, -\omega_z^R + \omega_x^R, -\omega_x^R - \omega_y^R)$
(1,1,0)	$(\omega_x^R, \omega_y^R, \omega_z^R)$	$(-(-1)^{i_x}\omega_x^{M_x}, -(-1)^{i_y}\omega_y^{M_y}, (-1)^{i_z}\omega_z^{M_z})$	$(-\omega_y^R + \omega_z^R, \omega_z^R - \omega_x^R, \omega_x^R + \omega_y^R)$
(0,1,1)	$(\omega_x^R, \omega_y^R, \omega_z^R)$	$((-1)^{i_x}\omega_x^{M_x}, -(-1)^{i_y}\omega_y^{M_y}, -(-1)^{i_z}\omega_z^{M_z})$	$(\omega_y^R + \omega_z^R, -\omega_z^R + \omega_x^R, \omega_x^R - \omega_y^R)$
(1,0,1)	$(\omega_x^R, \omega_y^R, \omega_z^R)$	$(-(-1)^{i_x}\omega_x^{M_x}, (-1)^{i_y}\omega_y^{M_y}, -(-1)^{i_z}\omega_z^{M_z})$	$(\omega_y^R - \omega_z^R, \omega_z^R + \omega_x^R, -\omega_x^R + \omega_y^R)$
(1,1,1)	$(-\omega_x^R, -\omega_y^R, -\omega_z^R)$	$((-1)^{i_x}\omega_x^{M_x}, (-1)^{i_y}\omega_y^{M_y}, (-1)^{i_z}\omega_z^{M_z})$	$(\omega_y^R + \omega_z^R, \omega_z^R + \omega_x^R, \omega_x^R + \omega_y^R)$

Supplementary Table V. Similar to Supplementary Table IV but derived from E_{10} and E_{11} mechanisms.

(l_x,l_y,l_z)	E_{10} $\propto (-1)^{i_x+i_y+i_z}$	E_{11} $\propto (-1)^{i_x+i_y+i_z}$
(0,0,0)	$(\omega_y^R + \omega_z^R, \omega_z^R + \omega_x^R, \omega_x^R + \omega_y^R)$	$((-1)^{i_y}\omega_y^{M_y} + (-1)^{i_z}\omega_z^{M_z}, (-1)^{i_x}\omega_x^{M_x} + (-1)^{i_z}\omega_z^{M_z}, (-1)^{i_x}\omega_x^{M_x} + (-1)^{i_y}\omega_y^{M_y})$
(1,0,0)	$(\omega_y^R + \omega_z^R, -\omega_z^R + \omega_x^R, \omega_x^R - \omega_y^R)$	$((-1)^{i_y}\omega_y^{M_y} + (-1)^{i_z}\omega_z^{M_z}, -(-1)^{i_x}\omega_x^{M_x} - (-1)^{i_z}\omega_z^{M_z}, -(-1)^{i_x}\omega_x^{M_x} - (-1)^{i_y}\omega_y^{M_y})$
(0,1,0)	$(\omega_y^R - \omega_z^R, \omega_z^R + \omega_x^R, -\omega_x^R + \omega_y^R)$	$(-(-1)^{i_y}\omega_y^{M_y} - (-1)^{i_z}\omega_z^{M_z}, (-1)^{i_x}\omega_x^{M_x} + (-1)^{i_z}\omega_z^{M_z}, -(-1)^{i_x}\omega_x^{M_x} - (-1)^{i_y}\omega_y^{M_y})$
(0,0,1)	$(-\omega_y^R + \omega_z^R, \omega_z^R - \omega_x^R, \omega_x^R + \omega_y^R)$	$(-(-1)^{i_y}\omega_y^{M_y} - (-1)^{i_z}\omega_z^{M_z}, -(-1)^{i_x}\omega_x^{M_x} - (-1)^{i_z}\omega_z^{M_z}, (-1)^{i_x}\omega_x^{M_x} + (-1)^{i_y}\omega_y^{M_y})$
(1,1,0)	$(\omega_y^R - \omega_z^R, -\omega_z^R + \omega_x^R, -\omega_x^R - \omega_y^R)$	$(-(-1)^{i_y}\omega_y^{M_y} - (-1)^{i_z}\omega_z^{M_z}, -(-1)^{i_x}\omega_x^{M_x} - (-1)^{i_z}\omega_z^{M_z}, (-1)^{i_x}\omega_x^{M_x} + (-1)^{i_y}\omega_y^{M_y})$
(0,1,1)	$(-\omega_y^R - \omega_z^R, \omega_z^R - \omega_x^R, -\omega_x^R + \omega_y^R)$	$((-1)^{i_y}\omega_y^{M_y} + (-1)^{i_z}\omega_z^{M_z}, -(-1)^{i_x}\omega_x^{M_x} - (-1)^{i_z}\omega_z^{M_z}, -(-1)^{i_x}\omega_x^{M_x} - (-1)^{i_y}\omega_y^{M_y})$
(1,0,1)	$(-\omega_y^R + \omega_z^R, -\omega_z^R - \omega_x^R, \omega_x^R - \omega_y^R)$	$(-(-1)^{i_y}\omega_y^{M_y} - (-1)^{i_z}\omega_z^{M_z}, (-1)^{i_x}\omega_x^{M_x} + (-1)^{i_z}\omega_z^{M_z}, -(-1)^{i_x}\omega_x^{M_x} - (-1)^{i_y}\omega_y^{M_y})$
(1,1,1)	$(-\omega_y^R - \omega_z^R, -\omega_z^R - \omega_x^R, -\omega_x^R - \omega_y^R)$	$((-1)^{i_y}\omega_y^{M_y} + (-1)^{i_z}\omega_z^{M_z}, (-1)^{i_x}\omega_x^{M_x} + (-1)^{i_z}\omega_z^{M_z}, (-1)^{i_x}\omega_x^{M_x} + (-1)^{i_y}\omega_y^{M_y})$

Supplementary Table VI. Similar to Supplementary Table IV but derived from E_{12} mechanism.

(l_x,l_y,l_z)	E_{12} $\propto (-1)^{i_x+i_y+i_z}$
(0,0,0)	$(-(-1)^{i_y}\omega_y^{M_y} - (-1)^{i_z}\omega_z^{M_z}, -(-1)^{i_x}\omega_x^{M_x} - (-1)^{i_z}\omega_z^{M_z}, -(-1)^{i_x}\omega_x^{M_x} - (-1)^{i_y}\omega_y^{M_y})$
(1,0,0)	$(-(-1)^{i_y}\omega_y^{M_y} - (-1)^{i_z}\omega_z^{M_z}, (-1)^{i_x}\omega_x^{M_x} + (-1)^{i_z}\omega_z^{M_z}, (-1)^{i_x}\omega_x^{M_x} + (-1)^{i_y}\omega_y^{M_y})$
(0,1,0)	$((-1)^{i_y}\omega_y^{M_y} + (-1)^{i_z}\omega_z^{M_z}, -(-1)^{i_x}\omega_x^{M_x} - (-1)^{i_z}\omega_z^{M_z}, +(-1)^{i_x}\omega_x^{M_x} + (-1)^{i_y}\omega_y^{M_y})$
(0,0,1)	$((-1)^{i_y}\omega_y^{M_y} + (-1)^{i_z}\omega_z^{M_z}, (-1)^{i_x}\omega_x^{M_x} + (-1)^{i_z}\omega_z^{M_z}, -(-1)^{i_x}\omega_x^{M_x} - (-1)^{i_y}\omega_y^{M_y})$
(1,1,0)	$((-1)^{i_y}\omega_y^{M_y} + (-1)^{i_z}\omega_z^{M_z}, (-1)^{i_x}\omega_x^{M_x} + (-1)^{i_z}\omega_z^{M_z}, -(-1)^{i_x}\omega_x^{M_x} - (-1)^{i_y}\omega_y^{M_y})$
(0,1,1)	$(-(-1)^{i_y}\omega_y^{M_y} - (-1)^{i_z}\omega_z^{M_z}, (-1)^{i_x}\omega_x^{M_x} + (-1)^{i_z}\omega_z^{M_z}, (-1)^{i_x}\omega_x^{M_x} + (-1)^{i_y}\omega_y^{M_y})$
(1,0,1)	$((-1)^{i_y}\omega_y^{M_y} + (-1)^{i_z}\omega_z^{M_z}, -(-1)^{i_x}\omega_x^{M_x} - (-1)^{i_z}\omega_z^{M_z}, (-1)^{i_x}\omega_x^{M_x} + (-1)^{i_y}\omega_y^{M_y})$
(1,1,1)	$(-(-1)^{i_y}\omega_y^{M_y} - (-1)^{i_z}\omega_z^{M_z}, -(-1)^{i_x}\omega_x^{M_x} - (-1)^{i_z}\omega_z^{M_z}, -(-1)^{i_x}\omega_x^{M_x} - (-1)^{i_y}\omega_y^{M_y})$

Supplementary Discussion V – The one-to-one correspondence between magnetic and electric DMI

We now discuss a bit on the transformations of the polar vectors $\mathbf{u}$ (e.g., the atomic displacement) and the axial vectors $\mathbf{m}$ (e.g., the magnetic moment) under the possible symmetric operations – the combination of proper rotations $\hat{\mathcal{C}}_\theta$, improper rotations $\hat{\mathcal{C}}_\theta\hat{\mathcal{I}}$, and translations $\hat{\tau}_{\mathbf{t}}$ – in 3-dimensional Euclidean space (for the details, see Ref. [13]). Note that all the symmetric operations of 3-dimensional Euclidean space can be generated by the three types of transformations $\hat{\mathcal{C}}_\theta$, $\hat{\mathcal{C}}_\theta\hat{\mathcal{I}}$, and $\hat{\tau}_{\mathbf{t}}$. Of course, we should include the time-reversal operation ($\hat{\mathcal{T}}$) as well. The proper rotation $\hat{\mathcal{C}}_\theta$ denotes the operation that rotates objects by θ angle along a certain axis [13]; the improper rotation $\hat{\mathcal{C}}_\theta\hat{\mathcal{I}}$ is proper rotation $\hat{\mathcal{C}}_\theta$ combined with inversion $\hat{\mathcal{I}}$ [13]; the translation $\hat{\tau}_{\mathbf{t}}$ has the following effect: $\hat{\tau}_{\mathbf{t}}\mathbf{r} \to \mathbf{r} + \mathbf{t}$ [13]. Note that the above mentioned θ and $\mathbf{t}$ can be arbitrary rotation angle and translation vector, respectively. The

transformation of polar and axial vectors (e.g., $\mathbf{u}$ and $\mathbf{m}$) are identical under pure rotational operations [14]. On the other hand, the improper rotations transform the polar and axial vectors in opposite ways [14]. For example, assuming that the inversion $\hat{\mathcal{I}}$ is centered on the origin of $\mathbf{u}$ and $\mathbf{m}$ vectors, then we have: $\hat{\mathcal{I}}\mathbf{u} \rightarrow -\mathbf{u}$ and $\hat{\mathcal{I}}\mathbf{m} \rightarrow \mathbf{m}$. An intuitive but not rigorous explanation is that the $\mathbf{u}$ is a displacement vector $\mathbf{r}$ which will obviously be reversed by inversion; while the $\mathbf{m}$, magnetic moment, is analogous to the angular momentum (say, the orbital angular momentum $\mathbf{L} = \mathbf{r} \times \mathbf{p}$) which is not reversed by inversion (note that under inversion, $\mathbf{r} \rightarrow -\mathbf{r}$, $\mathbf{p} \rightarrow -\mathbf{p}$, and therefore $\mathbf{r} \times \mathbf{p} \rightarrow \mathbf{r} \times \mathbf{p}$). Furthermore, the time-reversal $\hat{\mathcal{T}}$ leaves $\mathbf{u}$ invariant but transforms $\mathbf{m}$ to $-\mathbf{m}$. Now, let us analyze the transformation properties of $\mathbf{u}_i \times \mathbf{u}_j$ and $\mathbf{m}_i \times \mathbf{m}_j$. First, under $\hat{\mathcal{T}}$ we have $\mathbf{u}_i \rightarrow \mathbf{u}_i$, $\mathbf{u}_j \rightarrow \mathbf{u}_j$, $\mathbf{m}_i \rightarrow -\mathbf{m}_i$, and $\mathbf{m}_j \rightarrow -\mathbf{m}_j$. Consequently, both $\mathbf{u}_i \times \mathbf{u}_j$ and $\mathbf{m}_i \times \mathbf{m}_j$ remain invariant by $\hat{\mathcal{T}}$. Second, proper rotations and translations may shift the i and j sites to i' and j' sites, respectively, with (i', j') being identical or not-identical to (i, j); meanwhile, both of them have additional effects on the $\mathbf{u}$ and $\mathbf{m}$ vectors located at i or j sites; by proper rotations and translations the $\mathbf{u}$ and $\mathbf{m}$ vectors are transformed in the same way [14]. Overall, proper rotations and translations transforms $\mathbf{u}_i \times \mathbf{u}_j$ to $\mathbf{u'}_{i'} \times \mathbf{u'}_{j'}$ and $\mathbf{m}_i \times \mathbf{m}_j$ to $\mathbf{m'}_{i'} \times \mathbf{m'}_{j'}$ in a shared manner. Third, since the improper rotation $\hat{\mathcal{C}}_\theta\hat{\mathcal{I}}$ is the combination of $\hat{\mathcal{C}}_\theta$ and $\hat{\mathcal{I}}$, we only need to investigate the transformation properties of $\mathbf{u}_i \times \mathbf{u}_j$ and $\mathbf{m}_i \times \mathbf{m}_j$ under $\hat{\mathcal{I}}$. Similarly, we have: $\hat{\mathcal{I}}\mathbf{u}_i \times \mathbf{u}_j \rightarrow (-\mathbf{u}_{i'}) \times (-\mathbf{u}_{j'})$ and $\hat{\mathcal{I}}\mathbf{m}_i \times \mathbf{m}_j \rightarrow \mathbf{m}_{i'} \times \mathbf{m}_{j'}$, again, in a common manner. Hence, the transformation properties for $\mathbf{u}_i \times \mathbf{u}_j$ and $\mathbf{m}_i \times \mathbf{m}_j$ under the symmetry operations of 3-dimensional Euclidean space are exactly the same. The one-to-one correspondence between magnetic and electric DMI are thus established by the present work. In continuous model, the Néel- and Bloch-type magnetic Skyrmions are described by magnetic DMI given by $m_z(\nabla \cdot \mathbf{m}) - (\mathbf{m} \cdot \nabla)m_z$ [15, 16] and $\mathbf{m} \cdot (\nabla \times \mathbf{m})$ [15, 17], respectively ($\mathbf{m}$ and m_z being the magnetization vector and its z component). Based on our above analysis, it is natural to formulate the energetic terms, namely $u_z(\nabla \cdot \mathbf{u}) - (\mathbf{u} \cdot \nabla)u_z$ and $\mathbf{u} \cdot (\nabla \times \mathbf{u})$, for the electric Néel- and Bloch-type magnetic skyrmions. Note that the existence of $\mathbf{u} \cdot (\nabla \times \mathbf{u})$ and ferroelectric Bloch-type Skyrmions have been proposed by Ref. [18] as well. Let us end this section by emphasizing the one-to-one correspondence between magnetic and electric DMI. In other words, if a mechanism exists for magnetic (respectively, electric) DMI, a similar mechanism can work for electric (respectively, magnetic) DMI. One can thus naturally obtain the electric DMI mechanism by looking at the magnetic DMI term and replace the *dual* magnetic quantities (e.g., $\mathbf{m}_i$ and $\mathbf{m}_j$ in $\mathbf{D}_{ij} \cdot (\mathbf{m}_i \times \mathbf{m}_j)$, $\mathbf{m}$ and $\nabla \times \mathbf{m}$ in $\mathbf{m} \cdot (\nabla \times \mathbf{m})$) by *dual* electric quantities (e.g., $\mathbf{u}_i$ and $\mathbf{u}_j$, $\mathbf{u}$ and $\nabla \times \mathbf{u}$), and *vice versa*. The reason involving the *dual* magnetic/electric quantities for replacement is to maintain the inversion and time-reversal symmetry.

Supplementary Discussion VI – Other possible mechanisms for DMI

So far, we have taken perovskites as our platforms and highlighted the electric DMI which depends on in-phase or anti-phase tiltings; we have also shown that the electric and magnetic DMI present one-to-one correspondence in this case (note also that our above mentioned DMI are all site-dependent, see e.g., the $(-1)^{i_x+i_y+i_z}$ in Eq. S5). We are now wondering whether oxygen tiltings in perovskites are the unique factors to create the electric DMI, especially since it is well-known that the tiltings are not always the necessary conditions for *magnetic* DMI . This is evidenced by, e.g., the spin-current model for which the electric polarization is at the heart of the magnetic DMI [19]. We thus now aim at deriving and verifying another mechanism, involving the polarization, that may lead to electric DMI within the framework of tri-linear coupling and may be connected with the magnetic DMI based on the spin-current model. For simplicity, we assume that the polarization is homogeneous and oriented along the z direction (i.e., P_z) and we have also considered the q_{iz} $(i = 1, 2, 3, 4)$ order parameters defined in Supplementary Fig. 6. For lattices containing $4N$ in-plane B sites, the order parameters associated with q_{1z}, q_{2z}, q_{3z}, and q_{4z} modulations (see Supplementary Fig. 6) are given by

$$
\begin{aligned}
B_\alpha^{q_{1z}} &= \sum_{j_x}\sum_{j_y}[(-1)^{j_x}+1][(-1)^{j_y}+1](-1)^{(j_x+j_y)/2} r^B_{j_x,j_y,\alpha}/N \\
B_\alpha^{q_{2z}} &= \sum_{j_x}\sum_{j_y}[(-1)^{j_x+1}+1][(-1)^{j_y}+1](-1)^{(j_x+j_y-1)/2} r^B_{j_x,j_y,\alpha}/N \\
B_\alpha^{q_{3z}} &= \sum_{j_x}\sum_{j_y}[(-1)^{j_x}+1][(-1)^{j_y+1}+1](-1)^{(j_x+j_y-1)/2} r^B_{j_x,j_y,\alpha}/N \\
B_\alpha^{q_{4z}} &= \sum_{j_x}\sum_{j_y}[(-1)^{j_x+1}+1][(-1)^{j_y+1}+1](-1)^{(j_x+j_y-2)/2} r^B_{j_x,j_y,\alpha}/N
\end{aligned}
\tag{S7}
$$

where $r^{B}_{j_x,j_y\alpha}$ is the atomic displacement of B ion located at (j_x, j_y, j_z) site; note that we omit the site index j_z because the system is chosen to be homogeneous along z direction. We then derive an energetic term coupling the polarization and the $B^{q_{i\beta}}_{\alpha}$ as follows

$$\begin{aligned} E = P_z(&B^{q_{1z}}_{z}B^{q_{2z}}_{x} - B^{q_{1z}}_{x}B^{q_{2z}}_{z} + B^{q_{3z}}_{z}B^{q_{4z}}_{x} - B^{q_{3z}}_{x}B^{q_{4z}}_{z}) \\ -P_z(&-B^{q_{1z}}_{z}B^{q_{3z}}_{y} + B^{q_{1z}}_{y}B^{q_{3z}}_{z} - B^{q_{2z}}_{z}B^{q_{4z}}_{y} + B^{q_{2z}}_{y}B^{q_{4z}}_{z}) \end{aligned} \tag{S8}$$

Such analytical form is indeed an electric DMI induced by the electrical polarization! Note that Eqs. S8 and S4 can be used to derive the DMI vector induced by P_z, following the similar procedures and conventions in Supplementary Discussion IV. After some tedious but straightforward algebra, one can obtained the polarization-driven electric DMI as $D'(x)_y \propto P_z$, $D'(y)_x \propto -P_z$, and $D'(x)_x = D'(y)_y = 0$, with $D'(x)_y$, $D'(y)_x$, $D'(x)_x$ and $D'(y)_y$ having been defined in Supplementary Discussion IV (see the sentences after Eq. S3 and the caption of Supplementary Fig. 6). One can also easily demonstrate by cyclic permutations that, if the polarization is along the x- instead of the z-direction, one has $D'(y)_z \propto P_x$, $D'(z)_y \propto -P_x$, and $D'(y)_y = D'(z)_z = 0$. Similar ideas apply when the polarization is along y. It is straightforward as well to obtain the polarization mediated DMI when the polarization is along the pseudo-cubic [111] direction (e.g., $P_x = P_y = P_z$ for $R3c$ ferroelectrics).

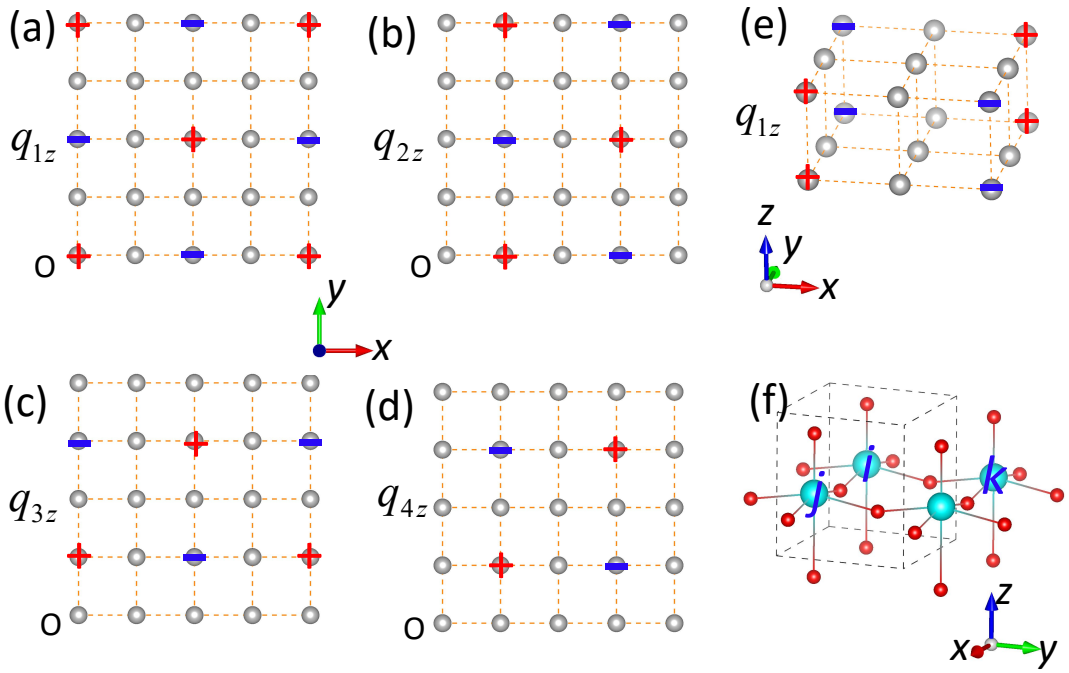

Supplementary Figure 6. Panels (a) to (d) are sketches of the q_{1z}, q_{2z}, q_{3z}, and q_{4z} modulations corresponding to ABO_3 perovskite. The "+" and "-" signs denote that the atomic displacement on that site are along positive (e.g., $+x$, $+y$, or $+z$) and negative (e.g., $-x$, $-y$, or $-z$) directions, respectively. Note that only the modulations within the $x-y$ plane are displayed; along z direction, the system is chosen to be homogeneous (see panel e). Panel (f) sketches the $P4mm$ structure of ABO_3 perovskite, that does not have BO_6 tilting but rather possesses a polarization contributed by B-site motions along the z direction. The electric DMI for $i-j$ and $i-k$ pairs are denoted by $\mathbf{D}'(x)$ and $\mathbf{D}'(y)$ vectors, respectively; for example, the x component of the DMI for $i-k$ pair is represented by $D'(y)_x$.

Let us now check numerically whether Eq. S8 is valid for an electric DMI. For that, we conduct DFT simulations using the VASP code and taking $BiAlO_3$ as an example. We start from the cubic perovskite $BiAlO_3$ ($a_{pc} = 3.82$ Å) and create a $4\times4\times1$ supercell. We impose the B^{Γ}_{z} component on Al sites with the magnitude of 0.04 a_{pc} and then create the $B^{q_{1z}}_{z}$ component on Al sites with varied magnitudes from -0.04 to 0.04 a_{pc} (B^{Γ}_{z} and $B^{q_{1z}}_{z}$ mimic the polarization and anti-polar motions, respectively). Consequently, we have $B^{q_{1z}}_{z}$ superimposed on B^{Γ}_{z}. We then found that DFT predicts that the forces acting on Al sites are associated with $B^{q_{2z}}_{x}$ and $B^{q_{3z}}_{y}$ configurations (see Supplementary Fig. 7), which

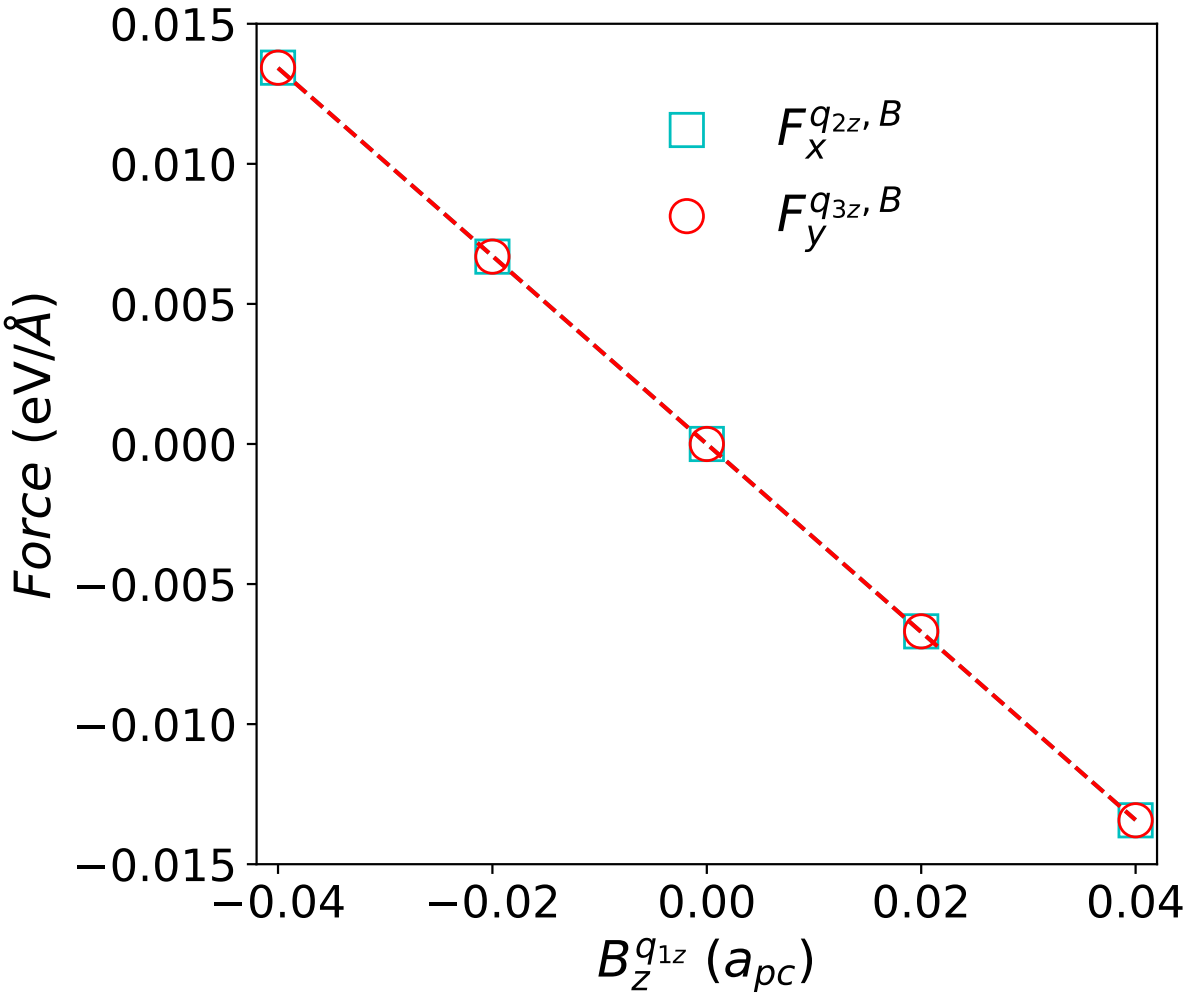

Supplementary Figure 7. The forces on Al ions (associated with $B_x^{Q_{2z}}$ and $B_y^{Q_{3z}}$ modulations) as a function of $B_z^{Q_{1z}}$ motions. Note that the B_z^{Γ} motions are fixed at 0.04 a_{pc}. See Text for details.

thus validates Eq. S8 and consequently validates an electric DMI that depends on polarization rather than tiltings! One can also easily prove that the electric DMI of Eq. S8 corresponds to the magnetic DMI associated with the spin-current model [20–22] by simply choosing the B quantities to be magnetic order parameters. For example, we can anticipate the magnetic DMI as $D(x)_y \propto P_z$, $D(y)_x \propto -P_z$, and $D(x)_x = D(y)_y = 0$ when the polarization is along the z-direction (e.g., P_z) – based on our established one-to-one correspondence between magnetic and electric DMI (see Supplementary Discussion V). It is now important to recall that, in the spin current model, the magnetic DMI is given by $\mathbf{D}_{ij} \propto \mathbf{P} \times \mathbf{e}_{ij}$ where $\mathbf{e}_{ij}$ is the unit vector pointing from i site to j site and $\mathbf{P}$ is the polarization vector [19–22]; with a polarization $P_z\mathbf{z}$ and a $\mathbf{e}_{ij} = \mathbf{x}$, the spin-current model will then give $\mathbf{D}_{ij} \propto P_z\mathbf{y}$ (e.g., $D(x)_y \propto P_z$); similarly, based on spin-current model, $P_z\mathbf{z}$ and $\mathbf{e}_{ik} = \mathbf{y}$ will yield $\mathbf{D}_{ik} \propto -P_z\mathbf{x}$ (e.g., $D(y)_x \propto -P_z$). Here, $\mathbf{x}$, $\mathbf{y}$, and $\mathbf{z}$ are unit vectors along x, y, and z directions (see e.g., Supplementary Fig. 6(f)). This totally coincides with our above analysis based on Eq. S8.

Let us now address another related topic. More precisely, in Ref. [18], the pseudo-Lifshitz term [17] $\mathbf{u} \cdot (\nabla \times \mathbf{u})$ was raised to predict the Bloch skyrmion in ferroelectric systems. Note that (1) such pseudo-Lifshitz term resides in the continuous model, while our proposed $\mathbf{D}'_{ij} \cdot (\mathbf{u}_i \times \mathbf{u}_j)$ is for a discrete model, and (2) the term in Ref. [18] was written as $u_z\partial u_x/\partial y - u_x\partial u_z/\partial y - u_z\partial u_y/\partial x + u_y\partial u_z/\partial x$, which is a special form of $\mathbf{u} \cdot (\nabla \times \mathbf{u})$; two other versions can be reached by doing the cyclic permutation (i.e., $(x, y, z) \to (y, z, x)$ and $(x, y, z) \to (z, x, y)$) as $u_x\partial u_y/\partial z - u_y\partial u_x/\partial z - u_x\partial u_z/\partial y + u_z\partial u_x/\partial y$ and $u_y\partial u_z/\partial x - u_z\partial u_y/\partial x - u_y\partial u_x/\partial z + u_x\partial u_y/\partial z$, respectively. The pseudo-Lifshitz term may hint a new mechanism of electric DMI (the so-called chiral DMI as proposed by Ref. [18]) that is also independent of the tiltings. Here, we shall just show that the pseudo-Lifshitz term do not apply to our considered mechanisms

which are mainly valid for non-collinear (anti-)ferroelectricity.

This is in fact readily to understand: $\mathbf{u}\cdot(\nabla\times\mathbf{u})$ can be null in our cases. As a matter of fact, let us take our trilinear coupling term $\omega_z^{M_z}B_x^{M_z}B_y^{\Gamma}$ as an example (see our E_5 term by assuming that $\boldsymbol{\omega}^M$ is along z direction). Here, $B_x^{M_z}$ and B_y^{Γ} indicate the M_z-point modulated anti-ferroelectric motions along x direction (say, $\mathbf{B}^{M_z}_{j_x,j_y,j_z}=(-1)^{j_x+j_y}b\ \mathbf{x}$) and weak ferroelectric motions along y direction (say, $\mathbf{B}^{\Gamma}_{j_x,j_y,j_z}=c\ \mathbf{y}$), respectively; b and c are constants (coefficients) and the integers j_x j_y and j_z label each site in B sublattice of ABO_3 perovskite. Note that we use $\mathbf{x}$, $\mathbf{y}$ and $\mathbf{z}$ to denote the unit vectors along x, y and z directions, respectively. As a result, the displacement field is given by $\mathbf{u}_{j_x,j_y,j_z}=\mathbf{B}^{M_z}_{j_x,j_y,j_z}+\mathbf{B}^{\Gamma}_{j_x,j_y,j_z}=(-1)^{j_x+j_y}b\ \mathbf{x}+c\ \mathbf{y}$. To connect the continuous model $\mathbf{u}\cdot(\nabla\times\mathbf{u})$ with our discrete case, we need to discretize the pseudo-Lifshitz term. For example, we have $\nabla\times\mathbf{u}\ \rightarrow\ (\frac{u_{j_x,j_y+1,j_z,z}-u_{j_x,j_y,j_z,z}}{j_y+1-j_y}-\frac{u_{j_x,j_y,j_z+1,y}-u_{j_x,j_y,j_z,y}}{j_z+1-j_z})\mathbf{x}+(\frac{u^{j_x,j_y,j_z+1,x}-u^{j_x,j_y,j_z,x}}{j_z+1-j_z}-\frac{u^{j_x+1,j_y,j_z,z}-u^{j_x,j_y,j_z,z}}{j_x+1-j_x})\mathbf{y}+(\frac{u^{j_x+1,j_y,j_z,y}-u^{j_x,j_y,j_z,y}}{j_x+1-j_x}-\frac{u^{j_x,j_y+1,j_z,x}-u^{j_x,j_y,j_z,x}}{j_y+1-j_y})\mathbf{z}=2(-1)^{j_x+j_y}b\ \mathbf{z}$ and $\mathbf{u}(\mathbf{r})\rightarrow\mathbf{u}_{j_x,j_y,j_z}=(-1)^{j_x+j_y}b\ \mathbf{x}+c\ \mathbf{y}$. Hence, $\mathbf{u}\cdot(\nabla\times\mathbf{u})$ is zero because $\nabla\times\mathbf{u}$ is along the z direction while $\mathbf{u}$ is within the $x-y$ plane. In addition, let us take a look at $u_z\partial u_x/\partial y-u_x\partial u_z/\partial y-u_z\partial u_y/\partial x+u_y\partial u_z/\partial x$ proposed in Ref. [18] and the two equivalent derivative versions obtained by cyclic permutations. We can soon realize that the discrete version of them also gives zero value because $\mathbf{u}_{j_x,j_y,j_z}=(-1)^{j_x+j_y}b\ \mathbf{x}+c\ \mathbf{y}$ has a null component along the z direction and the components along x and y directions do not depend on j_z.

Supplementary Discussion VII – A comparison between spin cantings driven by magnetic DMI and inhomogenous dipole patterns driven by electric DMI

In Supplementary Discussion IV, taking ABO_3 perovskite as our testing bed, we revealed the roles of BO_6 tilting as the source of a possible electric DMI. Based on the one-to-one correspondence, the magnetic DMI, microscopically originated from spin-orbit coupling, can be structurally rooted in the BO_6 tilting as well. For example, the z-oriented anti-phase BO_6 tiltings (i.e., ω_z^R) implies electric $D'(x)_z=(-1)^{i_x+i_y+i_z}K\omega_z^R$ (see Eq. S4) and magnetic $D(x)_z=(-1)^{i_x+i_y+i_z}\kappa\omega_z^R$, respectively. It is interesting to know the ratio $\frac{K}{\kappa}$, which is $\frac{D'(x)_z}{D(x)_z}$. Note that the spin (or magnetization) and dipole (or displacement) have different units (e.g., μ_B *vs* Å), so as $\mathbf{D'}$ and $\mathbf{D}$. It is thus in principle not possible to directly compare the magnetic and electric DMI strengths in a well-defined manner. However, based on the consequences arising from magnetic and electric DMI, the comparison can be fulfilled in some indirect ways. Indeed, in non-collinear magnetism and (anti-)ferroelectricity, the spin and dipole cantings can result from magnetic and electric DMI (see e.g., our mechanisms in Table I of the main text), respectively. We thus employ the magnetic $LaFeO_3$ system to test how strong is the electric DMI as compared to the magnetic DMI. Again, we start from the cubic $LaFeO_3$ with 40-atom supercell (e.g., $2\times2\times2$, $a=2a_{pc}=7.64$ Å), impose the various anti-phase tiltings about the z-axis (ω_z^R) from about -4.5 to 4.5 Degree; for each ω_z^R value, we then (1) create on Fe ions the $R-$point modulated (see Supplementary Table I, magnetic version of by B_x^R) predominant magnetic vectors along the x direction, and run non-collinear magnetic calculations including the spin-orbit coupling (self-consistent calculations without optimizing crystal structures), and (2) create on Fe ions the $R-$point modulated predominant displacement vectors along x direction (electric version of B_x^R), and structurally optimize – using selective dynamics methods in VASP – the other degrees of freedom but fix the oxygen positions, the Fe positions along the x axis as well as the lattice parameters (using $R-$point modulated scalar magnetism without including spin-orbit coupling).

The noncollinear magnetism calculations give a weak magnetism along the y directions (for the magnetic version of B_y^{Γ}). Similarly, the selective dynamics optimization results in weak ferroelectric motions along the y-direction (for the electric version of B_y^{Γ}). This again confirms the one-to-one correspondence between magnetic and electric DMI. Note that the dipole canting for $BiAlO_3$ in the presence of ω_z^R is further checked following a similar strategy used for $LaFeO_3$ based on PBEsol functional. It is worth emphasizing that the spin-canting angles in $LaFeO_3$ arises from two facts: the magnetic $\mathbf{D}_{ij}$ which favors the 90^0 or 270^0 between the angles of nearest-neighbor spin pairs $\mathbf{S}_i$ and $\mathbf{S}_j$ according to $\mathbf{D}_{ij}\cdot(\mathbf{S}_i\times\mathbf{S}_j)$, and the exchange interaction J_{ij} which favors the 180 or 0^0 between that of $\mathbf{S}_i$ and $\mathbf{S}_j$ by $J_{ij}\mathbf{S}_i\cdot\mathbf{S}_j$. Hence, the spin-canting angle is a measure of D/J (e.g., the ratio between DMI and exchange interaction). Similarly, in the electric counterpart, the electric version of exchange interaction J'_{ij} together with DMI $\mathbf{D}'_{ij}$ determines the dipole canting. Thus the dipole-canting angles reflects the electric ratio D'/J'. In other words, our above comparison between ω_z^R driven dipole and spin cantings, in fact, is a comparison between electric D'/J' and magnetic D/J (shown as Fig. 4 of the main text). The slope of lines in Fig. 4 of the main text, obtained by linear fitting, indicates the electric K/J' for $LaFeO_3$, electric K/J' $BiAlO_3$, and magnetic κ/J for $LaFeO_3$, respectively, with the values of 0.0067, 0.012, and 0.001 per Degree. Hence, the electric D'/J' can be much

larger than the magnetic D/J.

[1] Y. Yang, W. Ren, M. Stengel, X. H. Yan, and L. Bellaiche, Phys. Rev. Lett. **109**, 057602 (2012).
[2] A. A. Belik, S. Y. Stefanovich, B. I. Lazoryak, and E. Takayama-Muromachi, Chem. Mater. **18**, 1964 (2006).
[3] P. Chen, M. N. Grisolia, H. J. Zhao, O. E. González-Vázquez, L. Bellaiche, M. Bibes, B.-G. Liu, and J. Íñiguez, Phys. Rev. B **97**, 024113 (2018).
[4] L. Bellaiche and J. Íñiguez, Phys. Rev. B **88**, 014104 (2013).
[5] E. Bousquet, M. Dawber, N. Stucki, C. Lichtensteiger, P. Hermet, S. Gariglio, J.-M. Triscone, and P. Ghosez, Nature **452**, 732 (2008).
[6] N. A. Benedek and C. J. Fennie, Phys. Rev. Lett. **106**, 107204 (2011).
[7] A. T. Mulder, N. A. Benedek, J. M. Rondinelli, and C. J. Fennie, Adv. Funct. Mater. , 4810 (2013).
[8] J. M. Rondinelli and C. J. Fennie, Adv. Mater. **24**, 1961 (2012).
[9] H. J. Zhao, J. Íñiguez, W. Ren, X. M. Chen, and L. Bellaiche, Phys. Rev. B **89**, 174101 (2014).
[10] M. D. Peel, S. P. Thompson, A. Daoud-Aladine, S. E. Ashbrook, and P. Lightfoot, Inorg. Chem. **51**, 6876 (2012).
[11] L. Bellaiche, Z. Gui, and I. A. Kornev, J. Phys.: Condens. Matter **24**, 312201 (2012).
[12] H. J. Zhao, J. Íñiguez, X. M. Chen, and L. Bellaiche, Phys. Rev. B **93**, 014417 (2016).
[13] M. El-Batanouny and F. Wooten, *Symmetry and Condensed Matter Physics A Computational Approach* (Cambridge University Press, 2008).
[14] A. W. Joshi, *Elements of Group Theory for Physicists* (Wiley Eastern, 1984).
[15] A. N. Bogdanov and D. A. Yablonskii, Sov. Phys. JETP **68**, 101 (1989).
[16] X. S. Wang, H. Y. Yuan, and X. R. Wang, Commun. Phys. **1**, 31 (2018).
[17] L. D. Landau and E. M. Lifshitz, *Electrodynamics of Continuous Media* (Pergamon Press, 1984).
[18] K. C. Erb and J. Hlinka, Phys. Rev. B **102**, 024110 (2020).
[19] H. Katsura, N. Nagaosa, and A. V. Balatsky, Phys. Rev. Lett. **95**, 057205 (2005).
[20] B. Xu, B. Dupé, C. Xu, H. Xiang, and L. Bellaiche, Phys. Rev. B **98**, 184420 (2018).
[21] C. Xu, B. Xu, B. Dupé, and L. Bellaiche, Phys. Rev. B **99**, 104420 (2019).
[22] D. Rahmedov, D. Wang, J. Íñiguez, and L. Bellaiche, Phys. Rev. Lett. **109**, 037207 (2012).